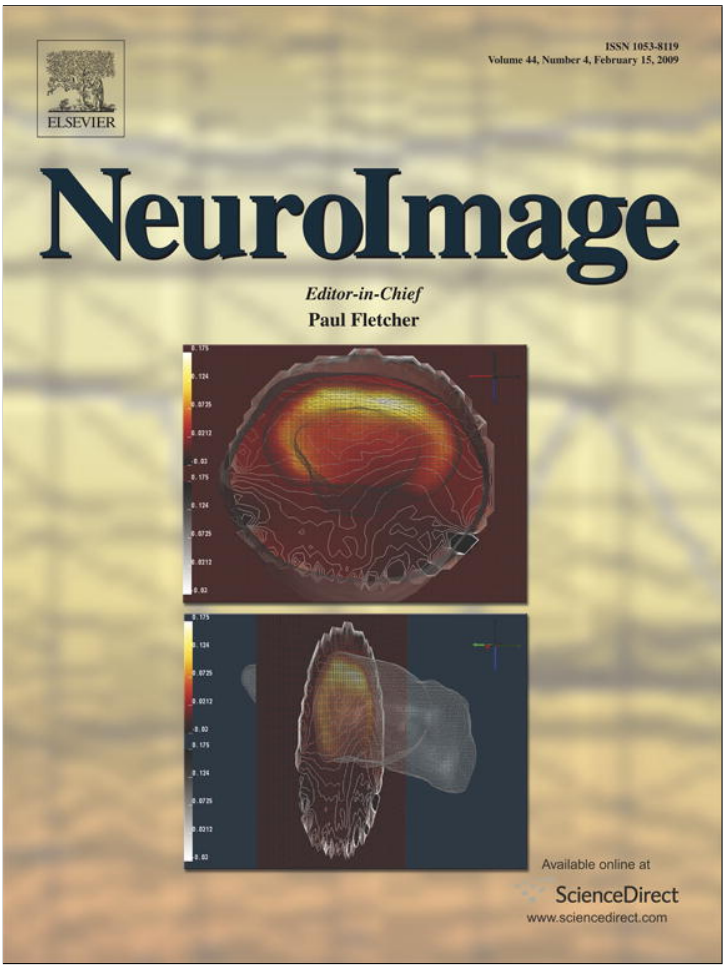

NeuroImage 44 (2009) 1415–1422

Contents lists available at ScienceDirect

NeuroImage

journal homepage: www.elsevier.com/locate/ynimg

Baseline and longitudinal patterns of brain atrophy in MCI patients, and their use in prediction of short-term conversion to AD: Results from ADNI ☆

Chandan Misra, Yong Fan, Christos Davatzikos *

Section of Biomedical Image Analysis, Department of Radiology, University of Pennsylvania, School of Medicine, 3600 Market Street, suite 380, Philadelphia, PA 19104, USA

ARTICLE INFO

Article history:
Received 24 July 2008
Revised 13 October 2008
Accepted 16 October 2008
Available online 5 November 2008

Keywords:
Alzheimer's disease
AD
Early detection
Mild cognitive impairment
MCI
Pattern classification
Structural MRI
Imaging biomarker

ABSTRACT

High-dimensional pattern classification was applied to baseline and multiple follow-up MRI scans of the Alzheimer's Disease Neuroimaging Initiative (ADNI) participants with mild cognitive impairment (MCI), in order to investigate the potential of predicting short-term conversion to Alzheimer's Disease (AD) on an individual basis. MCI participants that converted to AD (average follow-up 15 months) displayed significantly lower volumes in a number of grey matter (GM) regions, as well as in the white matter (WM). They also displayed more pronounced periventricular small-vessel pathology, as well as an increased rate of increase of such pathology. Individual person analysis was performed using a pattern classifier previously constructed from AD patients and cognitively normal (CN) individuals to yield an abnormality score that is positive for AD-like brains and negative otherwise. The abnormality scores measured from MCI non-converters (MCI-NC) followed a bimodal distribution, reflecting the heterogeneity of this group, whereas they were positive in almost all MCI converters (MCI-C), indicating extensive patterns of AD-like brain atrophy in almost all MCI-C. Both MCI subgroups had similar MMSE scores at baseline. A more specialized classifier constructed to differentiate converters from non-converters based on their baseline scans provided good classification accuracy reaching 81.5%, evaluated via cross-validation. These pattern classification schemes, which distill spatial patterns of atrophy to a single abnormality score, offer promise as biomarkers of AD and as predictors of subsequent clinical progression, on an individual patient basis.

Introduction

The most common cause of dementia is Alzheimer's disease, with incidence doubling approximately every 5 years after the age of 65. As life expectancy increases, AD is becoming an important health problem in the elderly, and a significant societal and financial burden. As many treatments are being developed and evaluated, it is becoming important to develop diagnostic and prognostic biomarkers that can predict which individuals are relatively more likely to progress clinically. This is especially important in individuals with MCI, who present a conversion rate of approximately 15% per year.

MCI has attracted a lot of attention in the recent years, in part because it offers opportunities for relatively early diagnosis of AD, and in part a number of pharmacological interventions typically target MCI patients. A number of studies, including both region-of-interest (ROI) and voxel-based analyses, have reported relatively reduced brain volumes in the hippocampus, parahippocampal gyrus, cingulate, and other brain regions in both MCI and AD patients (Jack et al., 1999, 2008; Karas et al., 2004; Fox and Schott, 2004; Chetelat et al., 2002; Convit et al., 2000; Dickerson et al., 2001; Kaye et al., 1997; Killiany et al., 2000; Stoub et al., 2005; Visser et al., 2002; De Leon et al., 2006). The spatial pattern of brain atrophy in MCI is complex and highly variable, and it evolves in time as the disease progresses. Therefore, capturing such spatio-temporal patterns of structural brain change requires sophisticated image analysis methods, including high-dimensional image warping often used to quantify the regional distribution of brain tissue. Even more challenging is the development of biomarkers that classify individuals, as opposed to characterizing group differences, as inter-individual variations and statistical overlap among groups renders it difficult to characterize individuals with sufficient sensitivity and specificity.

In order to be able to achieve individual classification, we leverage upon work on high-dimensional pattern classification that has shown great promise in the past 5 years as a means to measure subtle and spatially complex imaging patterns that have diagnostic value (Davatzikos et al., 2008a,b; Liu et al., 2004; Lao et al., 2003, 2004; Li et al., 2007; Adeli et al., 2005; Tandon et al., 2006, 2005; Kloppel et al., 2008a; Vemuri et al., 2008). This approach aims to provide computational tools that classify individuals, based on their imaging measurements, rather than determining statistical group differences. The

☆ Data used in the preparation of this article were obtained from the Alzheimer's Disease Neuroimaging Initiative (ADNI) database (www.loni.ucla.edu\ADNI). As such, the investigators within the ADNI contributed to the design and implementation of ADNI and/or provided data but did not participate in analysis or writing of this report. ADNI investigators include (complete listing available at http://www.loni.ucla.edu/ADNI/Data/ADNI_Manuscript_Citations.doc).

* Corresponding author.
E-mail address: christos@rad.upenn.edu (C. Davatzikos).

1053-8119/$ – see front matter © 2008 Elsevier Inc. All rights reserved.
doi:10.1016/j.neuroimage.2008.10.031

current study builds upon previous work in (Lao et al., 2004; Davatzikos et al., 2006; Fan et al., 2008a; Duchesne et al., 2008), by investigating longitudinal images from a relatively large sample of MCI individuals from ADNI. The primary goal of the current study is to utilize high-dimensional pattern classification of baseline scans to determine predictors of short-term conversion from MCI to AD. The secondary goal of this study is to measure the spatial distribution of brain atrophy, as well as its longitudinal change, in MCI converters (MCI-C) and in MCI non-converters (MCI-NC) in the ADNI cohort, and to evaluate differences between these two groups. The hypothesis was that advanced pattern analysis and classification techniques applied to baseline and longitudinal images of the regional distribution of brain tissues would allow us to predict future conversion from MCI to AD.

Materials and methods

ADNI

Data used in the preparation of this article were obtained from the ADNI database (www.loni.ucla.edu\ADNI). The goal of ADNI is to recruit 800 adults, ages 55 to 90, to participate in the research – approximately 200 CN older individuals to be followed for 3 years, 400 people with MCI to be followed for 3 years, and 200 people with early AD to be followed for 2 years. For up-to-date information see www.adni-info.org.

Participants

ADNI participants with structural MR images and at least one, in most cases two or more follow-up scans available on the ADNI web site as of March 2008 (the latest scan was from March 7, 2008) were part of this analysis; only scans that had undergone the various ADNI correction schemes were included, and for which at least a baseline and 2 follow-ups were available under the web site. This included 103 MCI participants (age range: 75.42±7.04), of which 27 (MCI-C, 77.04±5.95) were classified as having undergone conversion to AD based on changes in Global CDR from 0.5 to 1. The remaining 76 MCI participants (MCI-NC: 74.84±7.33) were classified as non-converters. The average time that elapsed between the baseline scans and conversion of MCI-C to AD was 15±6 (mean±std. deviation) months, and the average time interval between the baseline and first (last) follow-up scan was 0.67 (1.95) years. The MMSE scores (mean±std. deviation) of MCI-NC and MCI-C at baseline were 26.82±1.70 and 26.42±2.04, respectively. The groups were relatively well-matched in terms of gender (35.5% of MCI-C and 40.7% of MCI-NC were females).

Images

The datasets included standard T1-weighted images obtained using volumetric 3D MPRAGE or equivalent protocols with varying resolutions (typically 1.25×1.25 mm in-plane spatial resolution and 1.2 mm thick sagittal slices). Only images obtained using 1.5 T scanners were used in this study. The sagittal images were preprocessed according to a number of steps detailed under the ADNI website, which corrected for field inhomogeneities and image distortion, and were resliced to axial orientation.

Image analysis

Images were preprocessed according to previously validated and published techniques (Goldszal et al., 1998). The pre-processing steps included 1) Alignment to the AC–PC plane; 2) removal of extra-cranial material (skull-stripping); 3) Tissue segmentation into grey matter (GM), white matter (WM), and cerebrospinal fluid (CSF), using a brain tissue segmentation method proposed in (Pham and Prince, 1999); 4) High-dimensional image warping (Shen and Davatzikos, 2002) to a standardized coordinate system, a brain atlas (template) that was aligned with the MNI coordinate space (Kabani et al., 1998); 5) Formation of regional volumetric maps, named RAVENS maps (Goldszal et al., 1998; Davatzikos et al., 2001; Shen and Davatzikos, 2003), using tissue-preserving image warping (Goldszal et al., 1998). RAVENS maps quantify the regional distribution of GM, WM, and CSF, since one RAVENS map is formed for each tissue type. In particular, if the image warping transformation that registers an individual scan with the template applies an expansion to a GM structure, the GM density of the structure decreases accordingly to insure that the total amount of GM is preserved. Conversely, a RAVENS value increases during contraction, if tissue from a relatively larger region is compressed to fit a smaller region in the template. Consequently, RAVENS values in the template's (stereotaxic) space are directly proportional to the volume of the respective structures in the original brain scan. Therefore, regional volumetric measurements and comparisons are performed via measurements and comparisons of the respective RAVENS maps. For example, patterns of GM atrophy in the temporal lobe are quantified by patterns of RAVENS decrease in the temporal lobe in the stereotaxic space.

The RAVENS approach has been extensively validated (Goldszal et al., 1998; Davatzikos et al., 2001) and applied to a variety of studies (Resnick et al., 2000; Resnick et al., 2001; Kim et al., 2003; Resnick et al., 2003, 2004; Beresford et al., 2006a,b; Gur et al., 2006; Driscoll et al., 2007; Stewart et al., 2006). It uses a highly conforming high-dimensional image warping algorithm that captures fine structural details. Moreover, it uses tissue-preserving transformations, which ensures that image warping absolutely preserves the amount of GM, WM and CSF tissue present in an individual's scan, thereby allowing for local volumetric analysis.

In order to minimize longitudinal "jitter noise" that can be introduced by independently warping each person's image to the atlas, we first aligned all scans of each individual to his/her baseline scan, via rigid registration based on mutual information. We also minimized the potential biases that can be introduced by reslicing and interpolation, by reslicing each scan exactly one time: the baseline scans were resliced to be parallel to the AC–PC plane, and each follow-up was resliced in co-registration with the AC–PC aligned baseline scan of the respective participant.

Statistical analysis and pattern classification

Group comparisons were performed via voxel-based statistical analysis of respective RAVENS maps that were normalized by intracranial volume and smoothed using 8 mm full-width at half-maximum (FWHM) smoothing kernel. Group comparisons involved voxel-by-voxel *t*-tests applied by the SPM software (http://www.fil.ion.ucl.ac.uk/spm/software/spm5) to the RAVENS maps and to voxel-wise regression maps obtained from longitudinal RAVENS measurements. Group comparisons of the rates of change in the RAVENS maps, which reflect the rates of atrophy of respective tissue, were calculated by first applying voxel-wise linear regression to all available RAVENS maps of each participant, thereby obtaining a "beta" image of the rate of change for each participant, and subsequently applying SPM's *t*-test software.

In addition to the group analyses, we performed individual-patient analysis, aiming to classify individual scans belonging to MCI-C or MCI-NC participants based on their baseline MRI. This analysis is important because it directly relates to our ability to use quantitative MRI analysis for individual diagnosis, rather than to identify statistical differences between two potentially overlapping groups. Toward this end, we applied a high-dimensional pattern classification approach, which has been published and used in various neuroimaging studies (Fan et al., 2005; 2007, 2008a,b,c). This approach considers all brain regions jointly, and identifies a minimal set of brain regions/clusters whose volumes jointly maximally differentiate between the two

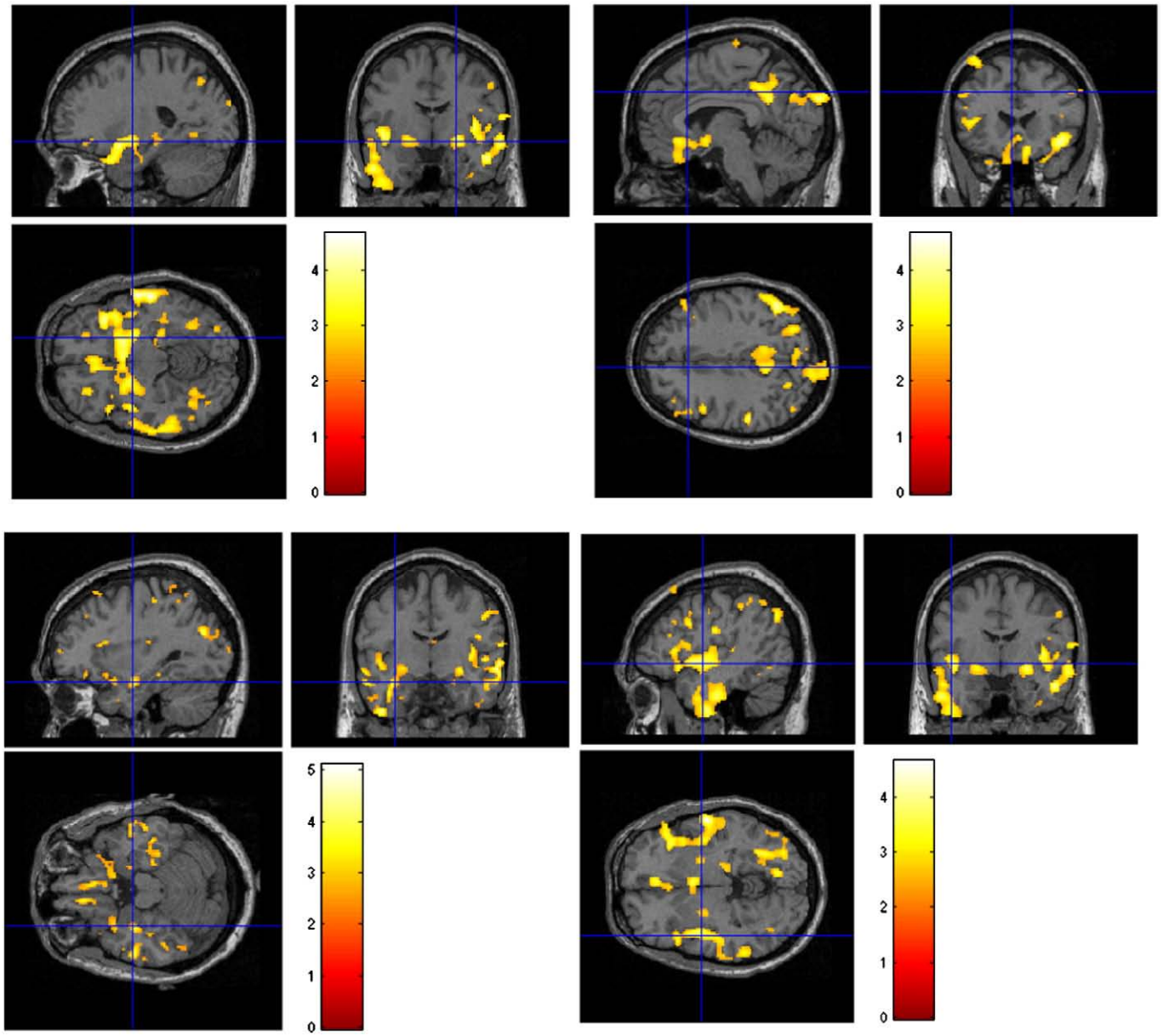

Fig. 1. Representative sections with regions of relatively reduced GM in MCI-C compared to MCI-NC, at baseline. The bottom-left *t*-maps were obtained by smoothing the RAVENS maps with a Gaussian kernel of 5 mm, to better display atrophy in the hippocampus. An 8 mm kernel was used in the top row of images. Images are in radiology convention. The scale indicates values of the *t*-statistic.

groups under consideration, on an individual scan basis; a detailed description can be found in (Fan et al., 2007a). Leave-one-out cross-validation is used to test this classification scheme on datasets not used for training, and obtain a relatively unbiased estimate of the generalization power of the classifier to new patients. The pattern classification method provides a *structural phenotypic score* (*SPS*). Two classifiers were constructed:

Classifier1: A classifier was constructed from the CN and AD groups that were described in detail in (Fan et al., 2008a) (including 66 CN individuals of mean age ± S.D., 75.18 ± 5.39 and 56 AD patients 77.40 ± 7.02 y.o.), and then applied to the MCI subjects. Positive SPS implies AD-like brain structure, and vice-versa. No cross-validation was necessary here, as the test sample (MCI) was different from the training sample (CN and AD).

Classifier2: A more specific classifier that optimally differentiates between MCI-C and MCI-NC was constructed and tested using leave-one-out cross-validation. In this process, all but one of the MCI participants are used to train a classifier that differentiates between the two groups. The resultant classifier is then applied to the left-out MCI subject. A positive SPS indicates a structural profile more similar to the converters, and vice versa. This process is repeated for all MCI subjects, thereby obtaining an estimate of the generalization ability of the classifier to new ("unseen" during training) samples.

Results

Voxel-based analysis of baseline RAVENS maps

Figs. 1–3 show representative sections obtained after applying voxel-wise *t*-tests to the baseline RAVENS maps of GM, WM and CSF. Several regions of relatively reduced volumes of GM in MCI-C compared to MCI-NC are evident, including the anterior hippocampus, amygdala, much of the temporal lobe GM and the insular cortex, posterior cingulate, and orbitofrontal cortex. WM was reduced

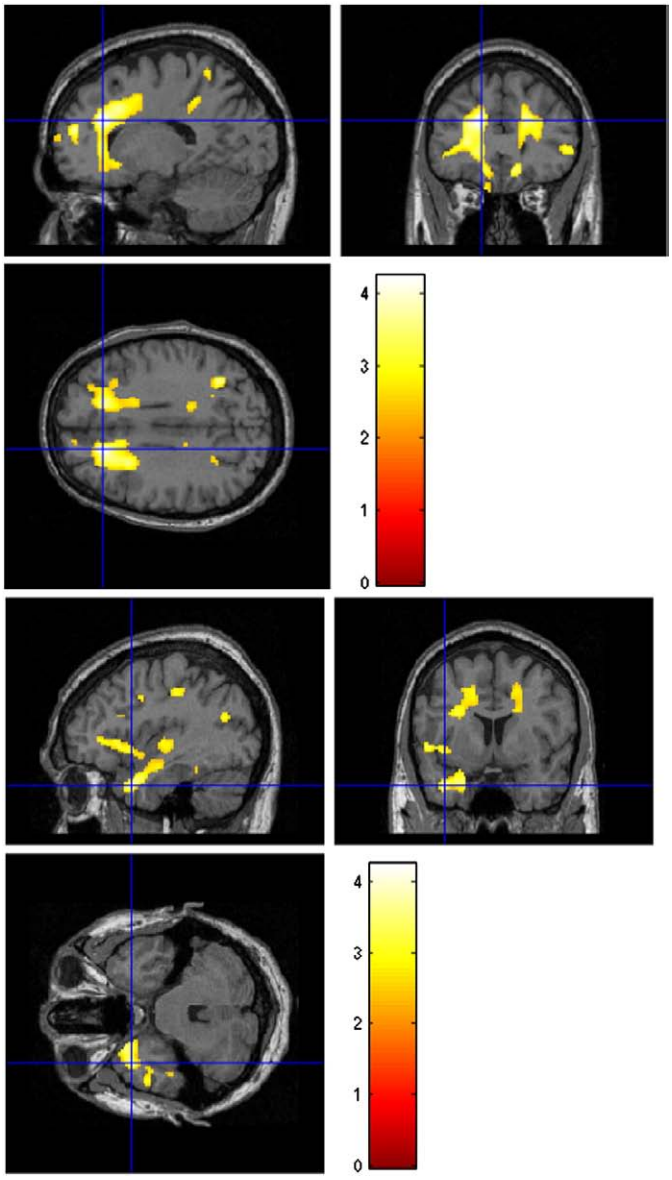

Fig. 2. Representative sections showing relatively reduced WM in MCI-C compared to MCI-NC, at baseline. Peri-ventricular WM loss is primarily due to periventricular leukoareosis, albeit it is also observed in peri-hippocampal inferio-medial locations. Images are in radiology convention. The scale indicates values of the *t*-statistic.

primarily in the periventricular frontal region, indicating higher periventricular leukoareosis in MCI-C compared to MCI-NC (in conjunction with the results of Fig. 4). WM was also relatively reduced in MCI-C anterior-laterally to the right hippocampus. Finally, ventricular CSF was relatively larger in the temporal horns of the lateral ventricles bilaterally. Regions of increased periventricular abnormal white matter in MCI-C, relative to MCI-NC, were also examined and are shown in Fig. 4, indicating relatively more pronounced leukoareosis in the former group.

Voxel-based analysis of regression maps of rate of RAVENS change

Relatively less pronounced were the differences in rate of change of GM, WM and CSF between the two MCI groups. Fig. 5 shows voxel-wise *t*-maps obtained from two-group comparisons of the rate of RAVENS change maps. We did not find any significant differences in the rates of change of GM and WM, other than a relatively faster increase of periventricular abnormal WM, especially in the vicinity of the temporal horns, indicating higher rates of development of leukoareosis in MCI-C. In the same regions, we also observed higher rates of CSF increase in MCI-C, indicating accelerating temporal horn enlargement in MCI-C.

AD-like patterns of atrophy in MCI individuals (Classifier1)

As described in the Materials and methods, a classifier that was previously constructed from the AD and CN individuals (Fan et al., 2008a) was applied to the current MCI sample; as reported in (Fan et al., 2008a), this classifier had achieved classification accuracy between AD and CN equal to 94.3%, evaluated via leave-one-out cross validation. Positive scores indicate AD-like brain structure and negative scores indicate normal structure. The average score of the MCI-C was 1.23±0.7 and of the MCI-NC was 0.46±1.28 (*p*-value of two-group *t*-test=0.0002). The histograms of the scores of these two MCI subgroups are shown in Fig. 6.

Pattern classification between MCI-C and MCI-NC (Classifier2)

As described in Materials and methods, we also constructed a classifier specifically targeting the best differentiation between MCI-C and MCI-NC. The classification accuracy as a function of the number of features (brain regions/clusters) for different kernel sizes is shown in Fig. 7. Maximum classification rate was 81.5%, however the classification rate tended to fluctuate between 75–80% for various numbers of features and kernel sizes. (Below a minimum number of features, performance decreased rapidly, as expected, since the spatial patterns were not properly sampled.) The receiver operating characteristic curve (ROC) reflecting the trade-off between sensitivity and specificity is shown in Fig. 8. The area under the curve (AUC) was 0.77.

Discussions and conclusion

This study utilized methods of computational neuroanatomy and high-dimensional pattern classification to investigate spatial patterns of brain atrophy, as well as their longitudinal change, in a group of 103 MCI individuals from the ADNI study, aiming to determine imaging markers that predict short-term conversion within a period of

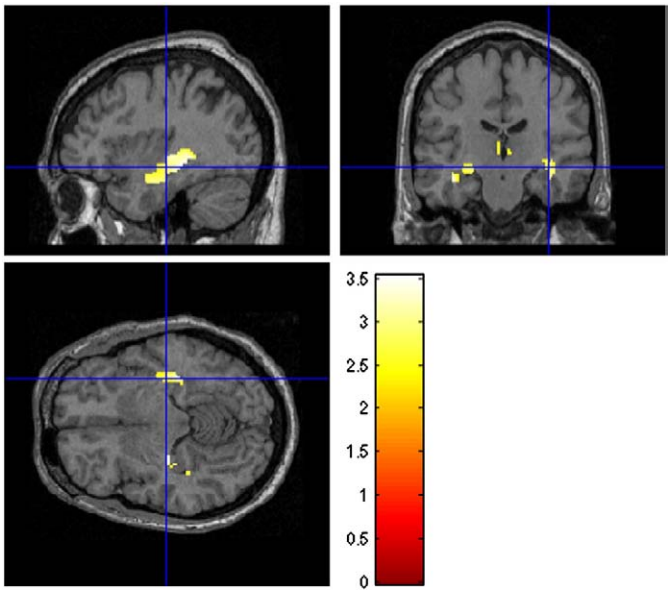

Fig. 3. Representative sections showing baseline ventricular enlargement in MCI-C compared to MCI-NC, primarily in the temporal horns. Images are in radiology convention. The scale indicates values of the *t*-statistic.

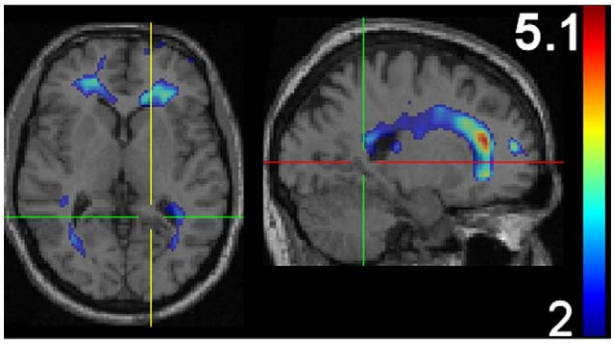

Fig. 4. Regions in which MCI-C had more baseline periventricular abnormal WM tissue, typical of leukoareosis. Images are in radiology convention. The scale indicates values of the *t*-statistic.

approximately 15 months, on average. Despite the relatively short clinical follow-up period of this study, significant differences at baseline were measured between MCI-C and MCI-NC. In particular, MCI-C had reduced GM volumes in a number of brain regions, including superior, middle and inferior temporal gyri, anterior hippocampus and amygdala, orbitofrontal cortex, posterior cingulate and the adjacent precuneous, insula, fusiform gyrus, and parahippocampal WM. Moreover, pronounced was the larger size of the temporal horns of the ventricles. It is therefore evident that MCI-C had already reached levels of widespread and significant brain atrophy at baseline. The short follow-up period further emphasizes the importance of this finding, since it is reasonable to assume that many of the MCI-NC are statistically expected to convert to AD in the near future, and are likely to also have significant and widespread atrophy at baseline.

The complexity of the pattern of differential atrophy between MCI-C and MCI-NC suggests that perhaps more sophisticated methods for measuring structural brain changes in MCI, AD, but also in normal aging, can be helpful for diagnosis and prognosis of the disease, compared to the most common approach that has been taken up to date in the neuroimaging literature (Chetelat et al., 2002; Convit et al., 2000; Dickerson et al., 2001; Kaye et al., 1997; Killiany et al., 2000), namely to examine volumes of a small number of structures typically of the hippocampus and the entorhinal cortex. This is further bolstered by histopathological studies (Braak et al., 1998) that have investigated the pattern of deposition of β-amyloid plaques and tau-pathology during the progression of AD, as well as with studies of magnetization transfer that indicated a more than expected widespread distribution of brain pathology (Van der Flier et al., 2002).

An important characteristic of this study is that, in addition to the group analysis, it also used individual patient classification using pattern recognition methods that have been extensively described and tested in the literature during the past few years (Lao et al., 2004; Vemuri et al., 2008; Fan et al., 2008a, b; Kloppel et al., 2008b). Thus, scores of AD-like patterns of brain atrophy were determined for each individual. The histogram of these scores (Fig. 6) clearly indicates that almost all MCI-C effectively had AD-like brains at baseline, since all but 2 scores were well into the positive range. This result agrees with growing evidence of the presence of significant AD pathology in many MCI patients (Kemppainen et al., 2007), and further amplifies the need to investigate the development of AD pathology at much earlier stages, ideally when individuals are cognitively normal. Recent studies have reported that very similar spatial patterns of brain atrophy develop in cognitive normal elderly and in very mild MCI individuals years before significant cognitive decline is evident clinically (Fan et al., 2007b, 2008b).

Further elaboration of the high-dimensional pattern classification technique, in which a classifier (Classifier 2) was constructed specifically to identify MCI-C on an individual basis, indicated that a relatively reasonable classification accuracy can be obtained (AUC = 0.77, maximum accuracy 81.5%), despite the fact that MCI-C and MCI-NC had about the same MMSE scores at baseline. In view of the heterogeneity of the MCI-NC group, which is reflected by the bi-modal distribution of the scores measuring AD-like atrophy (Fig. 6), this result is quite encouraging. Prediction of short-term conversion is important, as individuals classified as positive are likely to receive the most aggressive treatment. Moreover, it is clear from Fig. 6 that a number of MCI-NC have AD-like structural profiles, which indicates that these individuals might become converters soon. We are following the clinical data posted under the ADNI web site, and will report clinical progression in future studies.

In addition to the higher GM and WM atrophy, and ventricular enlargement found in MCI-C, we also found higher level of periventricular abnormal tissue, which appears gray in T1 images and is known to indicate small-vessel disease. The role of vascular disease in AD is receiving increasing attention in the literature (Troncoso et al., 2008; Snowdon et al., 1997; Schneider et al., 2003, 2004; Prins et al., 2004; Nihashi et al., 2001; Bennett et al., 2000; Shi et al., 2000; Lin et al., 1999a,b; Kim et al., 1998; De La Torre, 2004). Our results suggest that one of the significant differences between the MCI-C and MCI-NC subgroups is likely to be periventricular leukoareosis, and further support the need to examine vascular pathology in tandem with brain atrophy. Regardless of whether or not AD is pathophysiologically related to vascular disease, its clinical manifestation almost certainly depends on the concurrent presence of vascular disease (Troncoso et al., 2008; Schneider et al., 2004), therefore measuring vascular pathology is bound to be very important in predicting which individuals will convert to AD.

Against our expectation was the fact that the only significant group differences in the longitudinal rate of change were found in measures of periventricular abnormal WM and the temporal horn's CSF volumes. It is generally believed that rate of change is likely to be a better predictor of clinical progression. Although this might be the case in theory, practically obtaining robust measurements of rate of

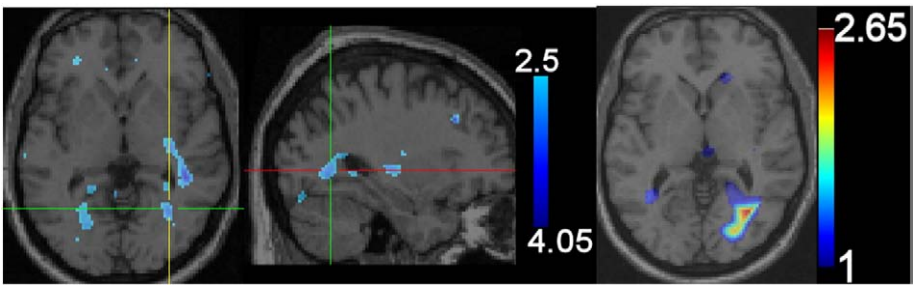

Fig. 5. Regions in which converters had most significant rates of tissue change compared to non-converters. Increases of GM (left) indicate progression of peri-ventricular leukoareosis. CSF increases (right) indicate rapid expansion of the temporal horns. Images are in radiology convention. The scale indicates values of the *t*-statistic.

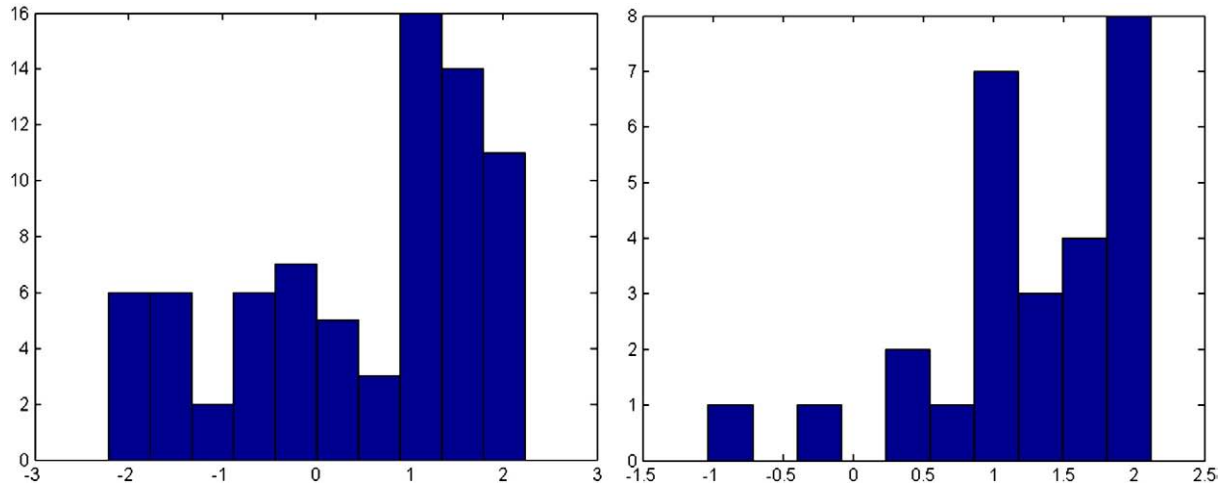

Fig. 6. Histograms of the structural abnormality scores for MCI-NC (left) and MCI-C (right). Positive implies AD-like structure whereas negative scores imply normal-like structure.

change from a limited number of imaging measurements is problematic, due to variations in scanner performance and tissue contrast, but also due to noise in the image analysis measurements, including segmentation and spatial normalization. Even though we used the ADNI data that has been corrected for scanner distortions, in this study we found that baseline measurements are far better markers of patterns of atrophy distinguishing converters from non-converters. To some extent this is expected, since baseline atrophy is the cumulative effect of possibly many years of progression of AD pathology. The use of high-dimensional pattern classification methods also helped amplify the predictive value of baseline measurements, since they allowed us to utilize nonlinear contrasts among regional volumetric measurements from many brain regions simultaneously to derive optimally differentiating directions in high-dimensional spaces, in which the two groups become highly separable. Rate of change is nonetheless a significant biomarker in clinical studies evaluating treatment effects.

The finding of reduced WM volumes between the two subgroups is interesting and merits further research, as it has been previously reported in studies comparing CN, AD and MCI in ADNI (Fan et al., 2008a). Although most WM reductions were periventricular, which agrees with the observed increase of abnormal periventricular tissue (Fig. 4), some inferior-medial temporal lobe regions also displayed reduced WM. Dense connections existing between the hippocampus and the posterior cingulate, which coupled with the early changes that have been reported in the posterior cingulate (Chetelat, 2003; Chetelat et al., 2003), might imply that changes in WM might provide additional markers of disease progression, something that has traditionally not attracted much attention in the AD literature. A growing recent literature using diffusion tensor imaging further supports the importance of examining white matter changes in AD (Naggara et al., 2006; Medina et al., 2006; Bozzali et al., 2002; Choi et al., 2005; Fellgiebel et al., 2004; Fellgiebel et al., 2005, 2006; Huang and Auchus, 2007; Moseley, 2002; Ray et al., 2006), albeit the majority of these studies have been restricted to measuring quantities such as fractional anisotropy and diffusivity, and therefore have not differentiated between brain atrophy and other tissue changes that can potentially have vascular underpinnings (for example, both fractional anisotropy and diffusivity are known to be lower in leukoareosis). More sophisticated types of analysis of diffusion tensor images (Verma and Davatzikos, 2006; Khurd et al., 2006) can potentially elucidate alterations of WM connectivity in AD.

In summary, we investigated the use of a high-dimensional pattern classification approach as a means to obtain a sensitive and specific biomarker of AD-like spatial patterns of brain atrophy, and of conversion from MCI to AD. The results of this short-follow-up study are encouraging and indicate that subtle and spatially complex patterns of brain atrophy can be detected and quantified with relatively high accuracy. Further follow-up will determine whether the baseline measurements can predict the time-to-conversion. Additional studies are required to test the generalization ability of this biomarker. However the fact that ADNI is a multi-center study, as well as the cross-validation used in our study, offer promise that this technology will prove to be robust across clinical sites.

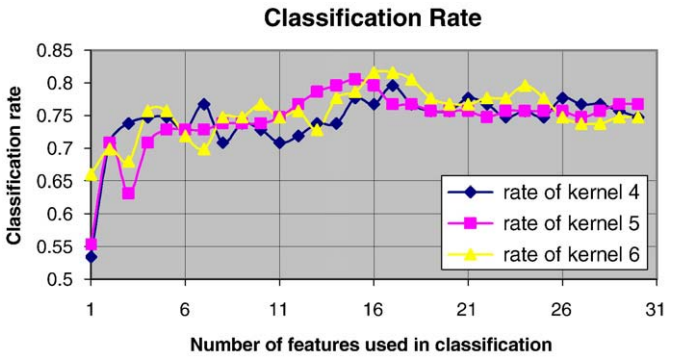

Fig. 7. Classification rate, evaluated via leave-one-out cross validation, between MCI-C and MCI-NC, as a function of the number of features (brain regions/clusters) used to build the classifier. Baseline images were used for classification.

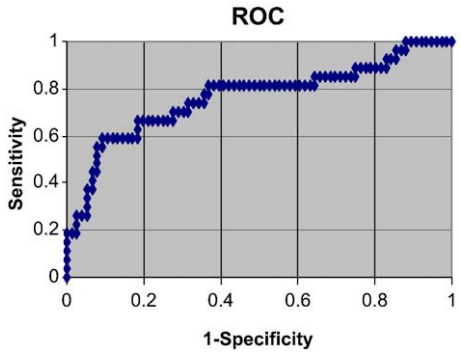

Fig. 8. ROC curve of the MCI-C vs. MCI-NC classification results of Fig. 7. Area under the curve = 0.77.

Acknowledgments

This study was financially supported by a grant by the Institute for the Study of Aging. Additional support was provided by the NIH grant R01AG14971. The authors would like to thank Evi Parmpi for help with data processing.

Data collection and sharing for this project was funded by the Alzheimer's Disease Neuroimaging Initiative (ADNI; Principal Investigator: Michael Weiner; NIH grant U01 AG024904). ADNI is funded by the National Institute on Aging, the National Institute of Biomedical Imaging and Bioengineering (NIBIB), and through generous contributions from the following: Pfizer Inc., Wyeth Research, Bristol-Myers Squibb, Eli Lilly and Company, GlaxoSmithKline, Merck and Co. Inc., AstraZeneca AB, Novartis Pharmaceuticals Corporation, Alzheimer's Association, Eisai Global Clinical Development, Elan Corporation plc, Forest Laboratories, and the Institute for the Study of Aging, with participation from the U.S. Food and Drug Administration. Industry partnerships are coordinated through the Foundation for the National Institutes of Health. The grantee organization is the Northern California Institute for Research and Education, and the study is coordinated by the Alzheimer's Disease Cooperative Study at the University of California, San Diego. ADNI data are disseminated by the Laboratory of NeuroImaging at the University of California, Los Angeles.

References

Adeli, H., Ghosh-Dastidar, S., Dadmehr, N., 2005. Alzheimer's disease and models of computation: imaging, classification, and neural models. J. Alzheimer's Dis. 7, 187–199.

Bennett, S.A.L., Pappas, B.A., Stevens, W.D., Davidson, C.M., Fortin, T., Chen, J., 2000. Cleavage of amyloid precursor protein elicited by chronic cerebral hypoperfusion. Neurobiol. Aging 21, 207–214.

Beresford, T., Arciniegas, D., Alfers, J., Clapp, L., Martin, B., Beresford, H., Du, Y., Liu, D., Shen, D., Davatzikos, C., Laudenslager, M., 2006a. Hypercortisolism in alcohol dependence and its relation to hippocampal volume loss. J. Stud. Alcohol 67, 861–867.

Beresford, T.P., Arciniegas, D.B., Alfers, J., Clapp, L., Martin, B., Du, Y., Liu, D., Shen, D., Davatzikos, C., 2006b. Hippocampus volume loss due to chronic heavy drinking. Alcohol., Clin. Exp. Res. 30, 1866–1870.

Bozzali, M., Falini, A., Franceschi, M., Cercignani, M., Zuffi, M., Scotti, G., Comi, G., Filippi, M., 2002. White matter damage in Alzheimer's disease assessed in vivo using diffusion tensor magnetic resonance imaging. J. Neurol. Neurosurg. Psychiatry 72, 742–746.

Braak, H., Braak, E., Bohl, J., Bratzke, H., 1998. Evolution of Alzheimer's disease related cortical lesions. J. Neural. Transm., Suppl. 54, 97–106.

Chetelat, G., 2003. Early diagnosis of Alzheiner's Disease: contribution of structural neuroimaging. NeuroImage 18, 525–541.

Chetelat, G., Desgranges, B., de la Sayette, V., Viader, F., Eustache, F., Baron, J.C., 2002. Mapping gray matter loss with voxel-based morphometry in mild cognitive impairment. NeuroReport 13, 1939–1943.

Chetelat, G., Desgranges, B., de la Sayette, V., Viader, F., Eustache, F., Baron, J.C., 2003. Mild cognitive impairment: can FDG-PET predict who is to rapidly convert to Alzheimer's disease? Neurology 60, 1374–1377.

Choi, S.J., Lim, K.O., Monteiro, I., Reisberg, B., 2005. Diffusion tensor imaging of frontal white matter microstructure in early Alzheimer's disease: a preliminary study. J. Geriatr. Psychiatry Neurol. 18, 12–19.

Convit, A., de Asis, J., de Leon, M.J., Tarshish, C.Y., De Santi, S., Rusinek, H., 2000. Atrophy of the medial occipitotemporal, inferior, and middle temporal gyri in non-demented elderly predict decline to Alzheimer's disease. Neurobiol. Aging 21, 19–26.

Davatzikos, C., Genc, A., Xu, D., Resnick, S.M., 2001. Voxel-based morphometry using the RAVENS maps: methods and validation using simulated longitudinal atrophy. NeuroImage 14, 1361–1369.

Davatzikos, C., Shen, D.G., Wu, X., Lao, Z., Hughett, P., Turetsky, B.I., Gur, R.C., Gur, R.E., 2005. Whole-brain morphometric study of schizophrenia reveals a spatially complex set of focal abnormalities. JAMA Arch. Gen. Psychiatry 62, 1218–1227.

Davatzikos, C., Resnick, S.M., Wu, X., Parmpi, P., Clark, C.M., 2008a. Individual patient diagnosis of AD and FTD via high-dimensional pattern classification of MRI. NeuroImage 41, 1220–1227.

Davatzikos, C., Fan, Y., Wu, X., Shen, D., Resnick, S.M., 2008b. Detection of prodromal Alzheimer's disease via pattern classification of magnetic resonance imaging. Neurobiol. Aging 29, 514–523 (electronic publication 2006).

De La Torre, J.C., 2004. Is Alzheimer's disease a neurodegenerative or a vascular disorder? Data, dogma, and dialectics. Lancet Neurol. 3, 184–190.

De Leon, M., DeSanti, S., Zinkowski, R., Mehta, P., Pratico, D., Segal, S., Rusinek, H., Li, J., Tsui, W., Louis, L.S., 2006. Longitudinal CSF and MRI biomarkers improve the diagnosis of mild cognitive impairment. Neurobiol. Aging 27, 394–401.

Dickerson, B.C., Goncharova, I., Sullivan, M.P., Forchetti, C., Wilson, R.S., Bennett, D.A., Beckett, L.A., deToledo-Morrell, L., 2001. MRI-derived entorhinal and hippocampal atrophy in incipient and very mild Alzheimer's disease. Neurobiol. Aging 22, 747–754.

Driscoll, I., Davatzikos, C., An, Y., Wu, X., Shen, D., Kraut, M., Resnick, S.M., 2007. Longitudinal brain changes in cognitively impaired and unimpaired older adults. presented at Society of neuroscience, San Diego, CA.

Duchesne, S., Caroli, A., Geroldi, C., Barillot, C., Frisoni, G.B., Collins, D.L., 2008. MRI-based automated computer classification of probable AD versus normal controls. IEEE Trans. Med. Imag. 27, 509–520.

Fan, Y., Shen, D., Davatzikos, C., 2005. Classification of structural images via high-dimensional image warping, robust feature extraction, and SVM. presented at MICCAI, Palm Springs, California, USA.

Fan, Y., Shen, D., Gur, R.C., Gur, R.E., Davatzikos, C., 2007a. COMPARE: classification of morphological patterns using adaptive regional elements. IEEE Trans. Med. Imag. 26, 93–105.

Fan, Y., Resnick, S.M., Shen, D., Kraut, M.A., Davatzikos, C., 2007b. MCI diagnosis via high-dimensional pattern classification with simultaneous utilization of MR and PET-CBF images yields 100% correct classification. presented at Alzheimer's Disease conference.

Fan, Y., Batmanghelich, N., Clark, C.M., Davatzikos, C., ADNI, 2008a. Spatial patterns of brain atrophy in MCI patients, identified via high-dimensional pattern classification, predict subsequent cognitive decline. NeuroImage 39, 1731–1743.

Fan, Y., Resnick, S.M., Wu, X., Davatzikos, C., 2008b. Structural and functional biomarkers of prodromal Alzheimer's disease: A high-dimensional pattern classification study. NeuroImage 41, 277–285 (Anatomy and Physiology Editors Choice Award 2008).

Fan, Y., Gur, R.E., Gur, R.C., Shen, D., Calkins, M.E., Davatzikos, C., 2008c. Unaffected family members and schizophrenia patients share brain structure patterns: a high-dimensional pattern classification study biological psychiatry. Biol. Psychiatry 63, 118–124.

Fellgiebel, A., Wille, P., Muller, M.J., Winterer, G., Scheurich, A., Vucurevic, G., Schmidt, L.G., Stoeter, P., 2004. Ultrastructural hippocampal and white matter alterations in mild cognitive impairment: a diffusion tensor imaging study. Dementia Geriatr. Cogn. Dis. 18, 101–108.

Fellgiebel, A., Muller, M.J., Wille, P., Dellani, P.R., Scheurich, A., Schmidt, L.G., Stoeter, P., 2005. Color-coded diffusion-tensor-imaging of posterior cingulate fiber tracts in mild cognitive impairment. Neurobiol. Aging 26, 1193–1198.

Fellgiebel, A., Dellani, P.R., Greverus, D., Scheurich, A., Stoeter, P., Muller, M.J., 2006. Predicting conversion to dementia in mild cognitive impairment by volumetric and diffusivity measurements of the hippocampus. Psychiatry Res. 146, 283–287.

Fox, N., Schott, J., 2004. Imaging cerebral atrophy: normal ageing to Alzheimer's disease. Lancet 363, 392–394.

Goldszal, A.F., Davatzikos, C., Pham, D., Yan, M., Bryan, R.N., Resnick, S.M., 1998. An image processing protocol for the analysis of MR images from an elderly population. J. Comput. Assist. Tomogr. 22, 827–837.

Gur, R., Davatzikos, C., Shen, D., Wu, X., Fan, Y., Hughett, P., Turetsky, B., Gur, R., 2006. Whole-brain deformation based morphometry MRI study of schizophrenia. Schizophr. Bull. 31, 408.

Huang, J., Auchus, A.P., 2007. Diffusion tensor imaging of normal appearing white matter and its correlation with cognitive functioning in mild cognitive impairment and Alzheimer's disease. Annals of New York Academy of Sciences 1097, 259–264.

Jack, C.R., Petersen, R.C., X.Y.C., O'Brien, P.C., Smith, G.E., Ivnik, R.J., Boeve, B.F., Waring, S. C., Tangalos, E., Kokmen, E., 1999. Prediction of AD with MRI-based hippocampal volume in mild cognitive impairment. Neurology 52, 1397–1403.

Jack, J.C.R., Weigand, S.D., Shiung, M.M., Przybelski, S.A., O'Brien, P.C., Gunter, J.L., Knopman, D.S., Boeve, B.F., Smith, G.E., Petersen, R.C., 2008. Atrophy rates accelerate in amnestic mild cognitive impairment. Neurology 70, 1740–1752.

Kabani, N., MacDonald, D., Holmes, C.J., Evans, A., 1998. A 3D atlas of the human brain. NeuroImage 7, S717.

Karas, G.B., Scheltens, P., Rombouts, S.A.R.B., Visser, P.J., Schijndel, R.A.v., Fox, N.C., Barkhof, F., 2004. Global and local gray matter loss in mild cognitive impairment and Alzheimer's disease. NeuroImage 23, 708–716.

Kaye, J., Swihart, T., Howieson, D., Dame, A., Moore, M., Karnos, T., Camicioli, R., Ball, M., Oken, B., Sexton, G., 1997. Volume loss of the hippocampus and temporal lobe in healthy elderly persons destined to develop dementia. Neurology 48, 1297–1304.

Kemppainen, N., Aalto, S., Wilson, I., Någren, K., Helin, S., Brück, A., Oikonen, V., Kailajärvi, M., Scheinin, M., Viitanen, M., Parkkola, R., Rinne, J., 2007. PET amyloid ligand [11C]PIB uptake is increased in mild cognitive impairment. Neurology 68, 1603–1606.

Khurd, P., Verma, R., Davatzikos, C., 2006. On characterizing and analyzing diffusion tensor images by learning their underlying manifold structure. presented at IEEE Computer Society Workshop on Mathematical Methods in Biomedical Image Analysis, Ney York, NY.

Killiany, R.J., Gomez-Isla, T., Moss, M., Kikinis, R., Sandor, T., Jolesz, F., Tanzi, R., Jones, K., Hyman, B.T., Albert, M.S., 2000. Use of structural magnetic resonance imaging to predict who will get Alzheimer's disease temporal lobe regions on magnetic resonance imaging identify patients with early Alzheimer's disease. Ann. Neurol. 47, 430–439.

Kim, H.S., Lee, S.H., Kim, S.S., Kim, Y.K., Jeong, S.J., Ma, J., Han, D.H., Cho, B.K., Suh, Y.H., 1998. Post-ischemic changes in the expression of Alzheimer's APP isoforms in rat cerebral cortex. NeuroReport 9, 533–537.

Kim, J.S., Kanaan, R., Kaufmann, W., Ross, C., Calhoun, V., Xu, D., Shen, D., Davatzikos, C., Godfrey Pearlson, G.D., 2003. Abnormal white matter organization in Huntington's disease evaluated with diffusion tensor MRI. presented at ISMRM, Toronto, Canada.

Kloppel, S., Stonnington, C.M., Chu, C., Draganski, B., Scahill, R.I., Rohrer, J.D., Fox, N.C., Jr, C.R.J., Ashburner, J., Frackowiak, R.S.J., 2008a. Automatic classification of MR scans in Alzheimer's disease. Brain.

Kloppel, S., Stonnington, C.M., Chu, C., Draganski, B., Scahill, R.I., Rohrer, J.D., Fox, N.C., Dummy Jr., C.R.J., Ashburner, J., Frackowiak, R.S.J., 2008. Automatic classification of MR scans in Alzheimer's disease. Brain 131, 681–689.

Lao, Z., Shen, D., Resnick, S., Davatzikos, C., 2003. Morphological classification of brains via high-dimensional shape transformations and machine learning methods. presented at Human Brain Mapping, New York City, USA.

Lao, Z., Shen, D., Xue, Z., Karacali, B., Resnick, S.M., Davatzikos, C., 2004. Morphological classification of brains via high-dimensional shape transformations and machine learning methods. NeuroImage 21, 46–57.

Lin, B., Schmidt-Kastner, R., Busto, R., Ginsberg, M.D., 1999a. Progressive parenchymal deposition of beta-amyloid precursor protein in rat brain following global cerebral ischemia. Acta Neuropathol. 97, 359–368.

Lin, B.W., Schmidt-Kastner, R., Busto, R., Ginsberg, X., 1999b. Progressive parenchymal deposition of beta-amyloid precursor protein immunoreactivity in rat brain following global cerebral ischemia. Stroke 30, 274.

Li, S., Shi, F., Pu, F., Li, X., Jiang, T., Xie, S., Wang, Y., 2007. Hippocampal shape analysis of Alzheimer disease based on machine learning methods. Am. J. Neuroradiol. 28, 1339–1345.

Liu, Y., Teverovskiy, L., Carmichael, O., Kikinis, R., Shenton, M., Carter, C.S., Stenger, V.A., Davis, S., Aizenstein, H., Becker, J., Lopez, O., Meltzer, C., 2004. Discriminative MR image feature analysis for automatic schizophrenia and Alzheimer's disease classification. presented at MICCAI, Saint-Malo, France.

Medina, D., deToledo-Morrell, L., Urresta, F., Gabrieli, J.D.E., Moseley, M., Fleischman, D., Bennett, D.A., Leurgans, S., Turner, D.A., Stebbins, G.T., 2006. White matter changes in mild cognitive impairment and AD: a diffusion tensor imaging study. Neurobiol. Aging 27, 663–672.

Moseley, M., 2002. Diffusion tensor imaging and aging — a review. NMR in Biomedicine 15, 553–560.

Naggara, O., Oppenheim, C., Rieu, D., Raoux, N., Rodrigo, S., Dalla Barba, G., Meder, J.F., 2006. Diffusion tensor imaging in early Alzheimer's disease. Psychiatry Res. Neuroimag. 146, 243–249.

Nihashi, T., Inao, S., Kajita, Y., Kawai, T., Sugimoto, T., Niwa, M., Kabeya, R., Hata, N., Hayashi, S., Yoshida, J., 2001. Expression and distribution of beta amyloid precursor protein and beta amyloid peptide in reactive astrocytes after transient middle cerebral artery occlusion. Acta Neurochir. 143, 287–295.

Pham, D.L., Prince, J.L., 1999. Adaptive fuzzy segmentation of magnetic resonance images. IEEE Trans. Med. Imag. 18, 737–752.

Prins, N.D., Dijk, E.J.v., Heijer, T.d., Vermeer, S.E., Koudstaal, P.J., Oudkerk, M., Hofman, A., Breteler, M.M.B., 2004. Cerebral white matter lesions and the risk of dementia. Arch. Neurol. 61, 1531–1534.

Ray, K.M., Wang, H., Chu, Y., Chen, Y.F., Bert, A., Hasso, A.N., Su, M.Y., 2006. Mild cognitive impairment: apparent diffusion coefficient in regional gray matter and white matter structures. Radiology 241, 197–205.

Resnick, S.M., Goldszal, A., Davatzikos, C., Golski, S., Kraut, M.A., Metter, E.J., Bryan, R.N., Zonderman, A.B., 2000. One-year age changes in MRI brain volumes in older adults. Cereb. Cortex 10, 464–472.

Resnick, S., Davatzikos, C., Kraut, M., Zonderman, A., 2001. Longitudinal changes in MRI volumes in older adults. Neurobiol. Aging 22, 5.

Resnick, S.M., Pham, D.L., Kraut, M.A., Zonderman, A.B., Davatzikos, C., 2003. Longitudinal magnetic resonance imaging studies of older adults: a shrinking brain. J. Neurosci. 23, 295–301.

Resnick, S., Pham, D., Davatzikos, C., Kraut, M., 2004. Sex differences in regional cerebral blood flow: clinical implications for Alzheimer's disease. Neurobiology of Aging 25, 263.

Schneider, J.A., Wilson, R.S., Cochran, E.J., Bienias, J.L., Arnold, S.E., Evans, D.A., Bennett, D.A., 2003. Relation of cerebral infarctions to dementia and cognitive function in older persons. Neurology 60, 1082–1088.

Schneider, J.A., Wilson, R.S., Bienias, J.L., Evans, D.A., Bennett, D.A., 2004. Cerebral infarctions and the likelihood of dementia from Alzheimer disease pathology. Neurology 62, 1148–1155.

Shen, D., Davatzikos, C., 2002. HAMMER: hierarchical attribute matching mechanism for elastic registration. IEEE Trans. Med. Imag. 21, 1421–1439.

Shen, D.G., Davatzikos, C., 2003. Very high resolution morphometry using mass-preserving deformations and HAMMER elastic registration. NeuroImage 18, 28–41.

Shi, J., Yang, S.H., Stubley, L., Day, A.L., Simpkins, J.W., 2000. Hypoperfusion induces overexpression of beta-amyloid precursor protein mRNA in a focal ischemic rodent model. Brain Res. 853, 1–4.

Snowdon, D.A., Greiner, L.H., Mortimer, J.A., Riley, K.P., Greiner, P.A., Markesbery, W.R., 1997. Brain infarction and the clinical expression of Alzheimer's disease. The Nun study. JAMA 277, 813–817.

Stewart, W.F., Schwartz, B.S., Davatzikos, C., Shen, D., Liu, D., Wu, X., Todd, A.C., Shi, W., Bassett, S., Youssem, D., 2006. Past adult lead exposure is linked to neurodegeneration measured by brain MRI. Neurology 66, 1476–1484.

Stoub, T.R., Bulgakova, M., Leurgans, S., Bennett, D.A., Fleischman, D., Turner, D.A., deToledo-Morrell, L., 2005. MRI predictors of risk of incident Alzheimer disease: a longitudinal study. Neurology 64, 1520–1524.

Tandon, R., Adak, S., Kaye, J., 2006. Neural networks for longitudinal studies in Alzheimer's disease. Artif. Intell. Med. 36, 245–255.

Troncoso, J.C., Zonderman, A.B., Resnick, S.M., Crain, B., Pletnikova, O., O'Brien, R.J., 2008. Effect of infarcts on dementia in the Baltimore longitudinal study of aging. Ann. Neurol.

Van der Flier, W.M.M., Van den Heuvel, D.M.J.M., Weverling-Rijnsburger, A.W.E.M., Spilt, A.M., Bollen, E.L.E.M., Westendorp, R.G.J., Middelkoop, H.A.M., Van Buchem, M.A., 2002. Cognitive decline in AD and mild cognitive impairment is associated with global brain damage. Neurology 59, 874–879.

Vemuri, P., Gunter, J.L., Senjem, M.L., Whitwell, J.L., Kantarci, K., Knopman, D.S., Boeve, B.F., Petersen, R.C., C.R.J., 2008. Alzheimer's disease diagnosis in individual subjects using structural MR images: validation studies. NeuroImage 39, 1186–1197.

Verma, R., Davatzikos, C., 2006. Manifold based analysis of diffusion tensor images using isomaps. presented at ISBI, Arlington, VA.

Visser, P.J., Verhey, F.R.J., Hofman, P.A., Scheltens, P., Jolles, J., 2002. Medial temporal lobe atrophy predicts Alzheimer's disease in patients with minor cognitive impairment. J. Neurol. Neurosurg. and Psychiatry 72, 491–497.